Effects of uniform injection at the wall on the stability of Couette-like flows

F. Nicoud and J. R. Angilella*
Centre Européen de Recherche et de Formation Avancée en Calcul Scientifique, 42 Avenue Gustave Coriolis, 31057 Toulouse Cedex, France
(Received 14 January 1997)

A linear stability analysis of a family of nearly parallel wall-bounded flows with injection at the lower wall and suction at the upper one is presented. The mean pressure gradient is such that the streamwise velocity profile remains linear in spite of injection. An asymptotic analysis shows that, for weak injection, the expansion rate of linear perturbations is a linear function of the injection Reynolds number (based on the width of the domain and the injection velocity). This point is confirmed by a numerical solver that also shows that, due to the injection process, the eigenmodes are drastically reorganized in the complex plane. In particular, the eigenvalue distribution is no longer symmetric. Moreover, the imaginary part of the phase velocity tends to increase so that some modes may become linearly unstable. However, the base flow remains stable as long as the injection Reynolds number is lower than a critical value close to 48. It is also found that higher injection rates (injection Reynolds numbers greater than 80) stabilize the flow, as already observed for channel or rotating flows. [S1063-651X(97)09309-4]

PACS number(s): 47.20.−k

I. INTRODUCTION

Wall-injected flows are of great interest in research as well as in industry and many experimental devices involve injection through a porous wall. They are also useful to mimic the effects of a transverse velocity component on a channel flow. For example, the combustion of a solid propellant inside a rocket motor creates a strong transverse component and the effects of this flux on the stability, the turbulence statistics, and the turbulence structure of the flow are not fully understood [1]. It is, however, shown [2] that the global stability of such a device is strongly related to the hydrodynamic stability of some sensible regions inside the combustion chamber. The present analysis is devoted to the understanding of the effect of injection on the linear stability of an elementary flow.

Changes in the turbulent fluxes for a flow submitted to slight wall injection are often accounted for by modifying the wall damping function [3]. Recently, direct numerical simulations of turbulent shear flows with wall injection show that turbulence statistics, as well as most of classical budgets, are modified near a porous wall [4,5]. The turbulence structure has also been shown in [1] to be drastically modified in the case of a large injection rate (injection velocity of the order of the wall shear velocity).

A linear stability analysis of an injection-induced flow in a planar porous-walled channel has been performed by Varapaev and Yagodkin [6]. The neutral stability curve that they obtained shows that the critical *axial-flow* Reynolds number (i.e., the axial-flow Reynolds number $R_{ax,ch}$ at which unstable modes may appear) is a linearly increasing function of the *injection* Reynolds number $R_{inj,ch}$ for $R_{inj,ch}$ greater than about 300. (The subscript ''ch'' denotes parameters corresponding to a *channel* with injection at both sides.) For low values of $R_{inj,ch}$, a reduction in the critical value of $R_{ax,ch}$ is observed, indicating that lower injection rates destabilize the flow. For higher values of $R_{inj,ch}$, the stability of the flow appreciably increases.

Other authors such as Chang and Sartory [7] as well as Min and Lueptow [8] have performed the linear stability analysis of the flow induced between two rotating permeable concentric cylinders when radial flow is present. It is shown in [8] that the Taylor number at which Taylor vortices appear decreases for small radial components. If the radial Reynolds number increases, the base flow becomes more stable because the outward flow overwhelms the centrifugal instability. In all cases, the Taylor vortices are shown to be shifted toward the outer cylinder by the radially outward flow.

In our analysis we consider a steady, fully developed (in the streamwise direction) flow of an incompressible fluid between two infinite porous plane walls, with uniform injection at the lower wall and opposite suction at the upper one. The lower wall is fixed, while the upper one moves along its own plane at a constant speed, and the streamwise pressure gradient is supposed to be constant. One of the most remarkable features of this flow is that, for large injection and suitable pressure gradient, it displays a steady boundary layer that is atypical in that its thickness is proportional to viscosity [9]. We focus on the case where the pressure gradient is fixed in such a way that the streamwise velocity profile is linear and the boundary layer vanishes. Very little is known about the stability of this flow. Following [10], we will investigate its linear stability by means of a normal-mode approach extended to nonparallel flows. This approach will enable us to generalize the analytical solution of [11] to the case of the wall-injected Couette flow.

This base flow, as well as the relevance of the normal modes approach, will be discussed precisely in the next section. The corresponding eigenvalue problem will be posed in Sec. III and partially solved in an analytical manner in Sec. IV under the assumption of low injection Reynolds number.

*Present address: Department of Applied Mathematics and Theoretical Physics, Silver Street, University of Cambridge, CB3 9EW Cambridge, United Kingdom.

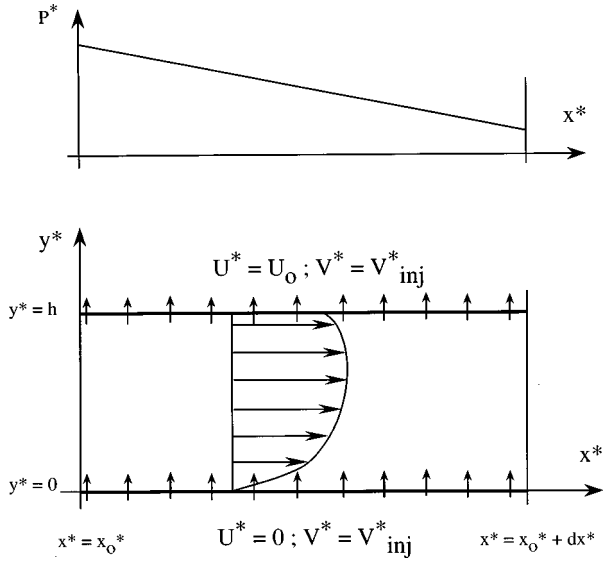

FIG. 1. Geometric configuration for the linear stability analysis. Since the flow is fully developed in the x^* direction, only the mean pressure varies along x^*, with a constant (negative) gradient.

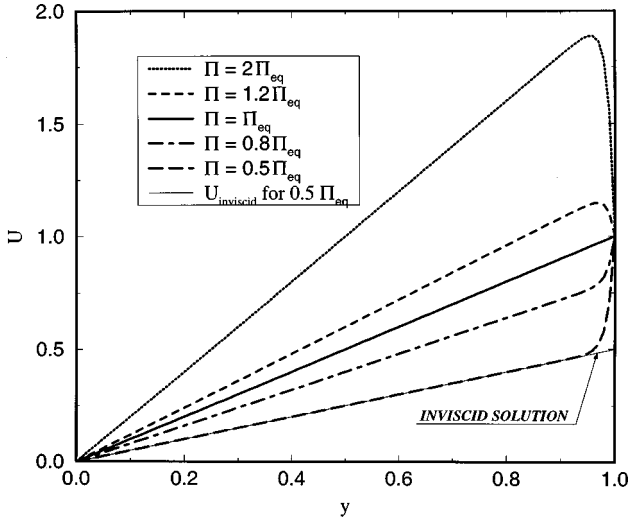

FIG. 2. Typical mean longitudinal velocity profiles for $R_{\text{inj}} = 85$ and different values of the pressure parameter Π. Note that the inviscid solution is valid in almost the whole domain for this injection Reynolds number.

The constants of the asymptotic models obtained are fixed using the numerical solver described in Sec. V. Finally, numerical results corresponding to higher injection rates are discussed in Sec. VI.

II. MEAN FLOW

Because the flow is fully developed in the x^* direction (all dimensional variables, except h and U_o, are noted with an asterisk superscript) and the fluid is incompressible, the mean velocity in the y^* direction V^* is constant and equals the injection or suction velocity V^*_{inj}. Furthermore, the dimensional mean streamwise velocity U^* depends only on the normal coordinate y^* and the mean pressure P^* is constant in the y^* direction. The gradient of P^* in the streamwise direction dP^*/dx^* is a fixed parameter of the flow. Since the lower wall ($y^*=0$) is fixed and the upper one ($y^*=h$) moves in its own plane at the constant streamwise speed U_o, the no-slip condition imposes $U^*=0$ for $y^*=0$ and $U^*=U_o$ for $y^*=h$. The flow geometry and the coordinate system are both described in Fig. 1.

Then, using h (the distance between the two walls) and U_o to nondimensionalize the x^*-momentum equation, we may obtain

$$\frac{R_{\text{inj}}}{R_o}\frac{dU}{dy}=\Pi+\frac{1}{R_o}\frac{d^2U}{dy^2}, \tag{1}$$

where Π is the nondimensional pressure gradient, defined as $\Pi=-(h/\rho U_o^2)(dP^*/dx^*)$. The Reynolds numbers R_o and R_{inj} are based on U_o and V^*_{inj}, respectively, and both on h. Classic no-slip boundary conditions are associated with Eq. (1):

$$U(0)=0, \quad U(1)=1. \tag{2}$$

The analytical solution of Eq. (1) with Eq. (2) may then be written as

$$U(y)=\Pi\,\frac{R_o}{R_{\text{inj}}}\,y+\left(1-\frac{\Pi R_o}{R_{\text{inj}}}\right)\frac{1-\exp R_{\text{inj}}y}{1-\exp R_{\text{inj}}}. \tag{3}$$

The first term on the right-hand side of Eq. (3) may be written as $U_{\text{inviscid}}=\Pi(U_o/V^*_{\text{inj}})y$. The solution of the inviscid problem with $V=V_{\text{inj}}$ at $y=0$ and $V=V_{\text{inj}}$ at $y=1$ is $U=U_{\text{inviscid}}$.

Clearly, an important value of Π is $\Pi_{\text{eq}}=R_{\text{inj}}/R_o$. For $\Pi=\Pi_{\text{eq}}$ the viscous solution (3) reduces to $U=U_{\text{inviscid}}$ and finally to $U=y$. If $0<\Pi<\Pi_{\text{eq}}$, the mean velocity induced by the favorable pressure gradient is small and a boundary layer develops near $y=1$. If $\Pi>\Pi_{\text{eq}}$ the pressure gradient effects are so important that U reaches a maximum greater than unity for $y<1$. A transition layer then allows U to reach unity when $y=1$. Various solutions are shown in Fig. 2 for different values of Π ($\Pi/\Pi_{\text{eq}}=2$, 1.2, 1, 0.8, and 0.5) and for $R_{\text{inj}}=85$. The inviscid solution is also plotted for $\Pi=0.5\Pi_{\text{eq}}$.

As already noted, if $\Pi=\Pi_{\text{eq}}=R_{\text{inj}}/R_o$, the mean longitudinal velocity remains linear and we obtain simply $U=y$. Thus the flow described by Eq. (3) with $\Pi=\Pi_{\text{eq}}$ is a generalized Couette flow *with injection and pressure gradient.* (The name ''Couette''is used here to refer to the classic form $U=y$ that is obtained.) Note that for a given outer Reynolds number R_o, when R_{inj} tends to zero, Π_{eq} also tends to zero and Eq. (3) corresponds to the classic parallel Couette flow without pressure gradient. In this paper, we carry out a linear stability analysis of the generalized Couette flow ($U=y$, $V=V_{\text{inj}}$, and $\Pi=R_{\text{inj}}/R_o$). Note that this flow may be seen as the limit of the flow studied by Min and Lueptow [8] when both the inner and outer radii of their cylindrical configuration tend to infinity and only the outer cylinder rotates about its axis. This latter case is equivalent to ours except that we consider a pressure gradient along the flow direction while these authors do not.

It is worth noting that the present flow is also strongly linked to the one studied by Varapaev and Yagodkin [6]. Indeed if $2H$ denotes the height of their channel with injec-

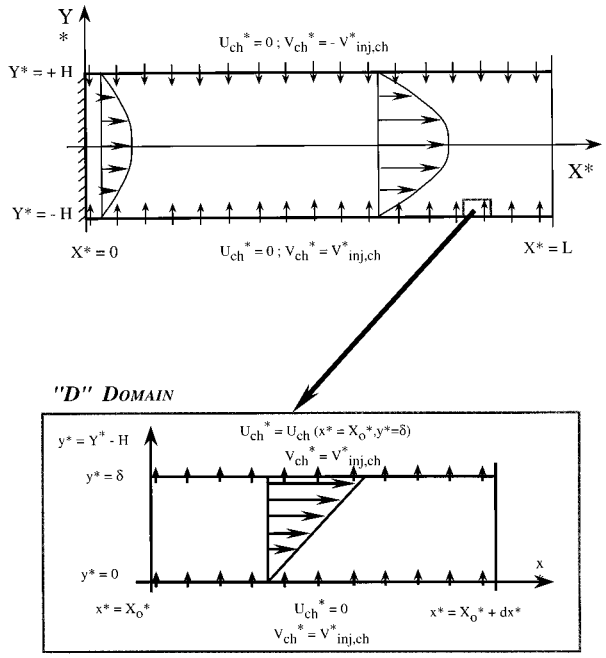

FIG. 3. Comparison of the generalized Couette flow (lower figure) and the channel with injection at both sides (upper figure). The former may be seen as a part of the latter.

tion at both sides (see Fig. 3), it is easy to show that the corresponding mean flow is such that

$$U^*_{\rm ch}=U^*_{\rm ax}\cos\left(\frac{\pi}{2}\frac{Y^*}{H}\right) \quad \text{with} \quad U^*_{\rm ax}=\frac{\pi V^*_{\rm inj,ch}}{2H}X^*, \tag{4}$$

$$V^*_{\rm ch}=V^*_{\rm inj,ch}\sin\left(\frac{\pi}{2}\frac{Y^*}{H}\right), \tag{5}$$

$$\frac{dP^*_{\rm ch}}{dX^*}=-\rho\left(\frac{\pi V^*_{\rm inj,ch}}{2H}\right)^2 X^*. \tag{6}$$

In these relations $U^*_{\rm ch}$, $V^*_{\rm ch}$ and $dP^*_{\rm ch}/dX^*$ denote the streamwise velocity, the normal (to the wall) velocity, and the streamwise pressure gradient, respectively. $U^*_{\rm ax}$ is the streamwise mean velocity at the center line of the channel ($Y^*=0$). X^* is the coordinate along the flow direction ($X^*=0$ at the front end of the channel). Note that Eqs. (4)–(6) are good approximations of the mean flow studied by Varapaev and Yagodkin [6] as long as the channel injection Reynolds number ($R_{\rm inj,ch}=V^*_{\rm inj,ch}H/\nu$) is large enough to allow the viscous terms to be neglected compared to the pressure effects. If this is not the case, the corresponding mean flow may still be derived analytically provided the front-end wall is replaced by a symmetry plane [12]. However, the corresponding velocity profile is not of cosine type anymore (it continuously passes from cosine to parabolic shape as $R_{\rm inj,ch}$ tends to zero).

Inside a small domain D defined by $-H\leqslant Y^*\leqslant -H+\delta$ and $X^*_o\leqslant X^*\leqslant X^*_o+dX^*$ with $\delta\ll H$ (see the exaggerated area of Fig. 3), the above mean quantities may be approximated as

$$U^*_{\rm ch}=U^*_{\rm ax}\frac{\pi}{2H}y^*, \tag{7}$$

$$V^*_{\rm ch}=V^*_{\rm inj,ch}, \tag{8}$$

$$\frac{dP^*_{\rm ch}}{dX^*}=-\rho\frac{U^*_{{\rm ch}(y^*=\delta)}V^*_{\rm inj,ch}}{\delta}. \tag{9}$$

In these relations, $y^*=Y^*+H$ and $y^*=0$ at the lower injection wall. If they are nondimensionalized using δ and $U^*_{{\rm ch}(y^*=\delta)}$, relations (8) and (9) define a flow that is equivalent to the base flow studied in the present paper ($U=y$, $V=V_{\rm inj,ch}$, and $\Pi=R_{\rm inj,ch}/R_{o,\rm ch}$). Here $R_{o,\rm ch}$ is an ''outer'' Reynolds number defined as $R_{o,\rm ch}=U^*_{{\rm ch}(y^*=\delta)}\delta/\nu$. Thus, *for high injection Reynolds numbers* $R_{\rm inj,ch}$, the generalized Couette flow corresponds to the near wall zone of Varapaev and Yagodkin's flow, that is to say, the linear part of their sine and cosine profiles for the normal and the streamwise velocity components. Recall that this is only the case when $R_{\rm inj,ch}$ is large enough (say, $R_{\rm inj,ch}>100$). Note also that the reference velocity $U^*_{{\rm ch}(y^*=\delta)}$ used to nondimensionalize relations (8) and (9) actually depend on the streamwise coordinate. As a consequence, the flow inside the domain D can be seen as a generalized Couette flow only if its length is small compared to its position X^*_o in the channel ($dX^*\ll X^*_o$).

III. EIGENVALUE PROBLEM

An important feature to note is that the generalized Couette flow (as defined in the preceding section) is nonparallel since it has a nonzero transverse component. As a consequence, the classical Orr-Sommerfeld equation for either parallel or nearly parallel flows [13] is not relevant for the present study. However, since the mean flow is periodic in the streamwise direction, the classic normal-mode approach [10] can be used to derive the relevant equation for the perturbations. The flow is defined with its stream function $\psi(x,y)$, separated into a mean and a fluctuating part

$$\psi(x,y)=\overline{\psi}(x,y)+\hat{\psi}(x,y,t). \tag{10}$$

In the context of *linear* stability analysis, the perturbation is supposed to be small so that the quadratic terms of fluctuating quantities are negligible compared to first-order terms. The starting point is the vorticity equation for two-dimensional incompressible flows

$$\Delta\psi_t+\psi_y(\Delta\psi)_x-\psi_x(\Delta\psi)_y=\frac{1}{R}\Delta(\Delta\psi), \tag{11}$$

where $R=U_{\rm ref}L_{\rm ref}/\nu$ is the Reynolds number based on a reference velocity $U_{\rm ref}$, length scale $L_{\rm ref}$, and the viscosity ν. (In the present study, we have chosen $U_{\rm ref}=U_o$ and $L_{\rm ref}=h$, so that R equals R_o.) The stream function has thus been nondimensionalized with $U_{\rm ref}L_{\rm ref}$. Using the normal-mode approach we write the perturbations in the form

$$\hat{\psi}(x,y,t)=\phi(y)\exp[i\alpha(x-ct)], \tag{12}$$

where α is real and denotes the spatial wave number of the perturbation; c is the complex phase velocity ($c=c_r+ic_i$, $i^2=-1$). This approach is valid for short times only since viscous and transverse effects rapidly change the shape of the perturbation amplitude ϕ.

Substituting Eq. (10) into Eq. (11), we obtain

$$U(\phi''-\alpha^2\phi)-\Delta U\phi+\frac{i}{\alpha R_o}(\phi^{(4)}-\alpha^2\phi'')-\frac{i}{\alpha}[V(\phi'''-\alpha^2\phi')-\Delta V\phi']=\left(c+\frac{i\alpha}{R_o}\right)(\phi''-\alpha^2\phi). \tag{13}$$

This is the well-known Orr-Sommerfeld equation in which an additional term due to the transverse mean flow appears. The mean flow is defined as

$$U(x,y)=\overline{\psi_y},\quad V(x,y)=-\overline{\psi_x}. \tag{14}$$

As already noted, if the mean flow is fully developed in the x direction, the mean normal velocity is constant because of continuity. If y varies in the (a,b) interval ($a=0$ and $b=1$ in our study), we set the boundary conditions

$$\phi(a)=\phi'(a)=\phi(b)=\phi'(b)=0, \tag{15}$$

which correspond to zero fluctuating velocities at the boundaries. Equation (13) with boundary conditions (15) defines an eigenvalue problem: We have to find combinations of (α,c,R_o) for which nontrivial solutions exist. We choose to study the *temporal* instability of the flow, so that we set α and R_o first and then solve Eq. (13) to obtain the solutions $[\phi(y)]$ and the corresponding complex phase velocity (c). The expansion rate of the perturbation is then $\omega=\alpha c_i$. It is positive if the flow is unstable for the wave number α and the Reynolds number R_o and negative if the flow is stable for these parameters.

IV. ASYMPTOTIC ANALYSIS

An asymptotic analysis based on the fact that injection is small compared to the streamwise velocity has been performed. Using Davey's methodology [11], we set

$$f(y)=\phi''(y)-\alpha^2\phi(y), \tag{16}$$

so that the stream function that satisfies $\phi'(1)=\phi(1)=0$ is

$$\phi(y)=\frac{-1}{\alpha}\int_y^1 \sinh[\alpha(y-s)]f(s)ds. \tag{17}$$

Equation (13) then reads

$$f''=\lambda^3(y-\overline{c})f+R_{\rm inj}f', \tag{18}$$

with $\lambda^3=i\alpha R_o$, the argument of λ is $\pi/6$, and $\overline{c}=c+i\alpha/R_o$. Solutions of Eq. (18) must satisfy boundary conditions at the wall: $\phi'(0)=\phi(0)=0$. We substitute these conditions into expression (17) to obtain

$$\int_0^1 \exp(\pm\alpha y)f(y)dy=0. \tag{19}$$

The only difference between Davey's problem and ours is the $R_{\rm inj}f'$ term in Eq. (18). We look for solutions of Eq. (18) of the form $f(y)=\int_C \exp[\lambda(y-\overline{c})t]g(t)dt$. This leads to

$$f(y)=\int_C \exp[\lambda(y-\overline{c})t+at^2-t^3/3]dt, \tag{20}$$

where $a=R_{\rm inj}/(2\lambda)$ and C is the classic complex contour used for the first Airy function $C=\{\infty\exp(i2\pi/3),\ \infty\exp(-i2\pi/3)\}$. Note that for $a=0$, Eq. (18) is the Airy equation and the solution is just $f(y)=\mathrm{Ai}[\lambda(y-\overline{c})]$. Writing Eq. (19) with expression (20) and assuming $\lambda\gg\alpha$, we obtain

$$\int_C \frac{\exp(\lambda t)-1}{t}\exp(bt+at^2-t^3/3)dt=0. \tag{21}$$

where $b=-\lambda\overline{c}$. Following Davey, we assume $|\lambda|\gg 1$ and write this equation to leading order in the form

$$F(a,b)=\int_C \frac{1}{t}\exp(bt+at^2-t^3/3)dt=0. \tag{22}$$

We shall discuss the reliability of this approximation later by examining the λ dependence of the obtained dispersion relations. The stability of the flow depends asymptotically on two complex parameters (a,b), i.e., on three real parameters $R_{\rm inj}/(\alpha R_o)^{1/3}$, c_r, and c_i. For $a=0$ the boundary condition (22) is just $A_1(b,1)=0$ (A_1 denotes the first generalized Airy function), which shows that b is constant, and leads to Davey's dispersion relations. For nonzero injections the roots of the $F(a,b)$ function are not known, but as F is continuously differentiable with respect to b, the implicit function theorem leads to

$$b=\tilde{F}(a), \tag{23}$$

where $\tilde{F}$ is a continuously differentiable function defined in an open neighborhood of a, which we denote $\mathcal{U}$. The third asymptotic hypothesis we use is that $R_{\rm inj}\ll(\alpha R_o)^{1/3}$ (i.e., a is close to 0), in such a way that $0\in\mathcal{U}$. As $\mathcal{U}$ is not empty ($\tilde{F}$ is not singular), this hypothesis is verified if a is small enough. The $\tilde{F}$ function can thus be approximated by its first-order Taylor series

$$\tilde{F}(a)\simeq\tilde{F}(0)+a\tilde{F}'(0). \tag{24}$$

We then obtain $b\simeq k_1+k_2a$, where k_1 and k_2 are complex constants. This leads to the dispersion relations

$$c_i\simeq-\frac{\alpha}{R_o}+\frac{A_0}{(\alpha R_o)^{1/3}}+A_1\frac{R_{\rm inj}}{(\alpha R_o)^{2/3}}, \tag{25}$$

$$c_r\simeq\frac{A_0'}{(\alpha R_o)^{1/3}}+A_1'\frac{R_{\rm inj}}{(\alpha R_o)^{2/3}}, \tag{26}$$

$$\alpha\ll(\alpha R_o)^{1/3}, \tag{27}$$

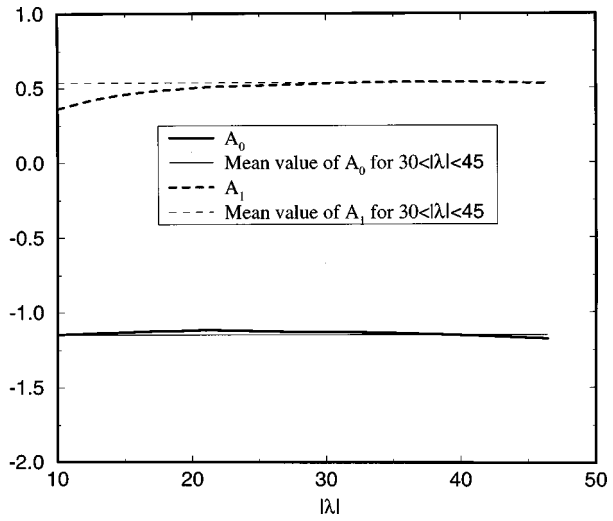

FIG. 4. Fitted constants versus $|\lambda|=(\alpha R_o)^{1/3}$. Note that the mean values used in the asymptotic model (see the text) are no longer valid for $|\lambda|<25$: for $|\lambda|=10$, the constant A_1 is only 0.37.

$$1 \ll (\alpha R_o)^{1/3}, \tag{28}$$

$$R_{\mathrm{inj}} \ll (\alpha R_o)^{1/3}. \tag{29}$$

Here A_0, A_1, A_0', and A_1' denote real constants. To estimate these constants, we made use of the numerical solver described in Sec. V. We find $A_0 \simeq -1.1$, in agreement with Davey's numerical fitting. Moreover, a positive value is found for A_1 ($A_1 \simeq 0.5$), showing that the injection term has a *destabilizing effect*, at least for small R_{inj}.

In order to test the reliability of the model we have examined the fitted constants A_0 and A_1, which are not expected to vary with λ. Figure 4 shows A_0 and A_1 versus $|\lambda|$ for $|\lambda| \in [10,46]$, obtained with $R_o \in [10^4,10^5]$, $\alpha=0.1$, and $\alpha=1$. For $\lambda<20$, the variation rate of A_1 is no longer negligible because the asymptotic hypothesis that simplifies Eq. (21) to Eq. (22) is no longer valid. Taking averaged values of A_0 and A_1 for $|\lambda| \in [30,45]$ (i.e., $\alpha R_o \in [27\,000,90\,000]$), a numerical dispersion relation for c_i is directly obtained from Eq. (25),

$$c_i \simeq -\frac{\alpha}{R_o} - \frac{1.1482}{(\alpha R_o)^{1/3}} + 0.5365\,\frac{R_{\mathrm{inj}}}{(\alpha R_o)^{2/3}}, \tag{30}$$

$$\alpha \ll (\alpha R_o)^{1/3}, \tag{31}$$

$$\alpha R_o \geqslant 27\,000, \tag{32}$$

$$R_{\mathrm{inj}} \ll (\alpha R_o)^{1/3}. \tag{33}$$

The third asymptotic assumption concerns the injection Reynolds number $R_{\mathrm{inj}} \ll (\alpha R_o)^{1/3}$. To estimate the values of R_{inj} for which this hypothesis is valid we have plotted c_i versus R_{inj} and compared numerical and analytical results (30). Figure 5 suggests that the model remains reliable for $R_{\mathrm{inj}} \sim 30$ and less, even if the asymptotic hypothesis $R_{\mathrm{inj}} \ll (\alpha R_o)^{1/3}$ is no longer valid, strictly speaking.

Higher-order asymptotic models are easily provided by the relation $b=\widetilde{F}(a)$. Indeed, since $\widetilde{F}$ is regular, Taylor's

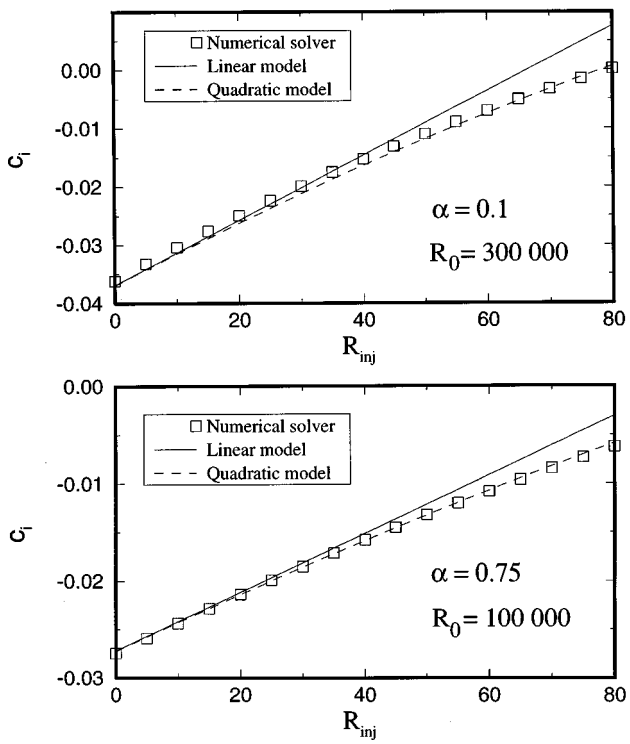

FIG. 5. Comparison between numerical results and the analytical dispersion relations corresponding to the linear and the quadratic models, for $\alpha R_o=30\,000$ and 75 000. The asymptotic assumption $R_{\mathrm{inj}} \ll (\alpha R_o)^{1/3}$ prevents the linear model from being reliable for $R_{\mathrm{inj}}>30$.

formula may be applied at higher order. For example, using a second-order approximation for $\widetilde{F}$,

$$\widetilde{F}(a) \simeq \widetilde{F}(0) + a\widetilde{F}'(0) + \frac{1}{2!}\,a^2\widetilde{F}''(0),$$

a quadratic dispersion relation is obtained:

$$c_i \simeq -\frac{\alpha}{R_o} - \frac{1.1482}{(\alpha R_o)^{1/3}} + 0.5365\,\frac{R_{\mathrm{inj}}}{(\alpha R_o)^{2/3}} - 0.0320\,\frac{R_{\mathrm{inj}}^2}{\alpha R_o}, \tag{34}$$

$$\alpha \ll (\alpha R_o)^{1/3}, \tag{35}$$

$$1 \ll (\alpha R_o)^{1/3}, \tag{36}$$

$$R_{\mathrm{inj}} \ll (\alpha R_o)^{1/3}. \tag{37}$$

As shown in Fig. 5, the analytical c_i steming from the latter model remains much closer to the numerical one. Anyway, as noticed for the first-order asymptotic formula, variation of A_1 with $|\lambda|$ discards those results if we move to another $|\lambda|$, especially if $|\lambda|<25$.

The main advantage of this asymptotic analysis is to show that, for small injection rates, the phase velocity of the most unstable mode is a linear function of the injection Reynolds number. However, this approach needed to be coupled with a numerical one in order to show that injection has a destabilizing effect. Moreover, the obtained dispersion relations are valid only in an open neighborhood of $a=0$ because the

implicit function theorem has been used. Consequently, it is worth continuing this study using the numerical tool already used to fit the constants A_0 and A_1. This tool is described in the next section.

V. NUMERICAL METHOD

In an attempt to investigate further the stability analysis of the so-called generalized Couette flow, a numerical solver for the Orr-Sommerfeld equation has been developed. In order to use the same solver for any mean flow, a finite-difference method has been chosen. It is slower than methods based on expansion in orthogonal functions [14], but can be easily applied to two-dimensional flows and does not depend on the mean profile we use. We suppose the flow is fully developed in the x direction, so that Eq. (13) only contains functions of the y variable. This implies that the y component of the mean flow is uniform. The y axis is discretized with N grid points:

$$y_i = a + (i-1)\,\frac{b-a}{N-1}, \quad i = 1, \ldots, N. \tag{38}$$

The amplitude of the fluctuating stream function is sampled $[\phi_i = \phi(y_i)]$ and its derivatives $\phi^{(n)} = (\phi_1^{(n)}, \ldots, \phi_N^{(n)})^T$ are given by a compact scheme [15]

$$A_n \phi^{(n)} = B_n \phi. \tag{39}$$

A_n is the $N \times N$ tridiagonal matrix of the compact scheme and B_n is an $N \times N$ banded matrix whose bandwidth depends on the stencil of the finite-difference method we choose (see Ref. [15]).

Equation (13) discretized with this method leads to

$$A\phi = \lambda B \phi, \tag{40}$$

with

$$\begin{aligned} A = {} & \mathrm{Diag}(U)(A_2^{-1}B_2 - \alpha^2 I) - \mathrm{Diag}(U'') \\ & + \frac{i}{\alpha R_o}\,(A_4^{-1}B_4 - \alpha^2 A_2^{-1}B_2) - \frac{i}{\alpha}\,\mathrm{Diag}(V) \\ & \times (A_3^{-1}B_3 - \alpha^2 A_1^{-1}B_1), \end{aligned} \tag{41}$$

$$B = A_2^{-1}B_2 - \alpha^2 I, \tag{42}$$

$$\lambda = c + \frac{i\alpha}{R_o}, \tag{43}$$

where $\mathrm{Diag}(f)$ is a diagonal matrix defined as

$$[\mathrm{Diag}(f)]_{i,j} = \delta_{i,j} f(y_i), \quad i = 1, \ldots, N.$$

Boundary conditions are imposed in an explicit manner, using a fourth-order finite-difference formula for ϕ'. On the lower boundary (a) we have

$$\begin{aligned} & \phi(a) = 0 \Rightarrow \phi_1 = 0, \\ & \phi'(a) = 0 \Rightarrow g(\phi_2, \phi_3, \phi_4, \phi_5) = 0, \end{aligned} \tag{44}$$

while for the upper boundary (b)

$$\begin{aligned} & \phi(b) = 0 \Rightarrow \phi_N = 0, \\ & \phi'(b) = 0 \Rightarrow g(\phi_{N-1}, \phi_{N-2}, \phi_{N-3}, \phi_{N-4}) = 0. \end{aligned} \tag{45}$$

Equations (44) and (45) provide a way to calculate $(\phi_1, \phi_2, \phi_{N-1}, \phi_N)$, so that we restrict the dimension of the eigenvalues problem (40)

$$\phi = (\phi_3, \ldots, \phi_{N-2})^T.$$

Then A and B denote $(N-4)\times(N-4)$ banded nonsymmetric matrices where the first (and last) two lines have been removed and lines near the boundaries have been modified according to Eqs. (44) and (45). Equation (40) defines a generalized eigenvalue problem, which we have solved with the LAPACK library.

The numerical procedure has been tested extensively for fundamental parallel flows (mixing layer, Couette flow, and Poiseuille flow) and quasiparallel flows (symmetric or asymmetric jets and channel flow with injection). The results obtained for the configuration studied in this paper (see Sec. II) are presented in the next section.

VI. NUMERICAL RESULTS

The numerical procedure described above has been used to study the influence of injection on the stability of the generalized Couette flow. In most computations, Eq. (13) has been discretized using 100 points in the y direction.

A. Eigenmodes

The influence of injection on the eigenmodes has been investigated. Its effect is clearly visible as mode locations drastically change in the (c_r, c_i) plane (this graph is often called the *spectrum* of the corresponding matrix by linear algebra specialists; this name, which may also be found in [13], will be used below). Typical mode distributions are plotted in Fig. 6. In this figure, filled and open symbols, as well as dots, denote eigenvalues. The injection Reynolds number lies in the range 0–200, and (R_o, α) is fixed (these values have been chosen according to an analysis of this flow performed in the turbulent case by Nicoud *et al.* [16]): $R_o = 3000$ and $\alpha = 1$. The filled circles denote the modes for zero injection Reynolds numbers, whereas the open symbols correspond to non-zero injection rates [$R_{\mathrm{inj}} = 50$ (circles), $R_{\mathrm{inj}} = 100$ (squares), $R_{\mathrm{inj}} = 150$ (diamonds), and $R_{\mathrm{inj}} = 200$ (triangles), respectively]. The path of a given mode, when injection increases, is given by dots in the (c_r, c_i) plane. For each path, the difference in R_{inj} between two consecutive dots is 1. Only the upper part $(c_i > -0.5)$ of the spectra is shown in Fig. 6 because it contains the most interesting modes (the modes likely to become unstable). For zero injection (filled circles), well-known results for parallel Couette flow without pressure gradient and injection are found. Since this flow is stable, all the modes are situated in the half plane corresponding to $c_i < 0$. Note also that real parts (c_r) of the modes lie in the interval $(U_{\min}, U_{\max}) = (0,1)$, in agreement with Joseph's theorem [17]. Finally, the mode repartition is symmetric with respect to the line $c_r = (U_{\max} + U_{\min})/2 = \frac{1}{2}$. It has been checked that the eigenvectors ϕ^+

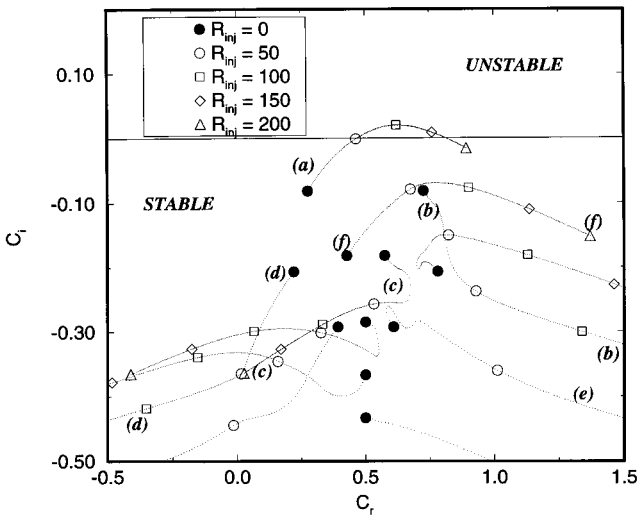

FIG. 6. Less stable eigenmodes for $R_o=3000$, $\alpha=1$, and $c_i>0.5$, with $0<R_{\text{inj}}<200$. The change in R_{inj} between two consecutive dots is 1. For no injection, the spectrum is symmetric and c_r lies in the range $U_{\min}$–$U_{\max}$, in agreement with Joseph's theorem. Injection makes modes spread out in the complex plane. When R_{inj} increases from 0, mode (a) becomes unstable and then stabilizes for $R_{\text{inj}}>170$.

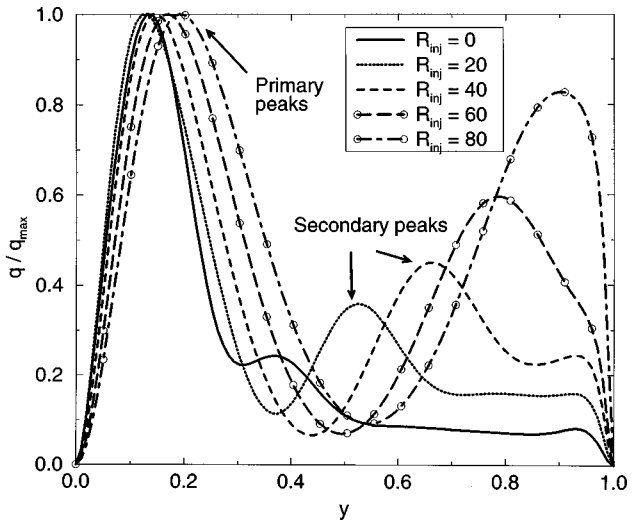

FIG. 7. Mean-kinetic-energy profiles for mode (a). Circles denote unstable modes. For each R_{inj}, q has been scaled by its maximal value. Note that the secondary peak approaches the upper wall when injection increases.

and ϕ^- associated with two symmetric eigenmodes c^+ and c^- $(c_i^+=c_i^-,\ c_r^+=1-c_r^-)$ are such that $\phi^+(y)=\phi^-(1-y)$.

When injection occurs, the modes are spread out across the spectrum, which is no longer symmetric. This is intuitively understable since, due to transverse convection, the base flow is not symmetric with respect to the line $y=0.5$. We can also note from Fig. 6 that the real part of the phase velocity may lie outside the range $U_{\min}$–$U_{\max}$ for R_{inj} of order 50 or greater [see modes (b), (d), and (e), for example]. This in not in disagreement with Joseph's theorem [17] since it has been derived for parallel flows only. The evolution of a given mode may be highly irregular when injection increases. For example, mode (e) follows a path whose direction changes rapidly three times between $R_{\text{inj}}=0$ and $R_{\text{inj}}\simeq 30$. Moreover, the distance between two consecutive dots (on a given path) may vary in a large extent [see mode (c) in Fig. 6]. This means that the phase velocity of the corresponding mode is not a linear function of the injection Reynolds number. However, for low R_{inj}, the evolution of the phase velocity of each mode is regular in the (c_r,c_i) plane. This result is in agreement with the linear (with respect to R_{inj}) dispersion relations (25)–(29), resulting from the asymptotic model derived in Sec. IV. Mode (a), which was one of the two most unstable modes of the flow without injection, becomes unstable immediately after $R_{\text{inj}}=50$. When R_{inj} increases further, the amplification rate of this mode increases too, up to $\alpha c_i\simeq 0.02$ for $R_{\text{inj}}\simeq 100$. Then injection begins to stabilize this mode and finally the base flow becomes stable again for $R_{\text{inj}}\simeq 170$. Recall that this feature (destabilization for low injection, stabilization for high injection rates) has already been observed by Varapaev and Yagodkin [6] and Min and Lueptow [8] for other mean flows. This result will be obtained for other α and R_o in Sec. VI C. Finally, note that mode (b) [the symmetric mode of (a) for the classic Couette flow] is never destabilized by injection. Its amplification rate decreases even for small values of R_{inj}, while that of mode (a) begins to grow. The following subsection is devoted to the comparison of the eigenvectors corresponding to paths (a) and (b).

B. Eigenvectors

Figures 7 and 8 show the mean-kinetic-energy profile $q(y)$ for the perturbations corresponding to modes (a) and (b) respectively. This quantity has been calculated by averaging the kinetic energy of the perturbations over a period:

$$q=\frac{1}{2}\frac{\alpha}{2\pi}\int_0^{2\pi/\alpha}(u^2+v^2)dx. \tag{46}$$

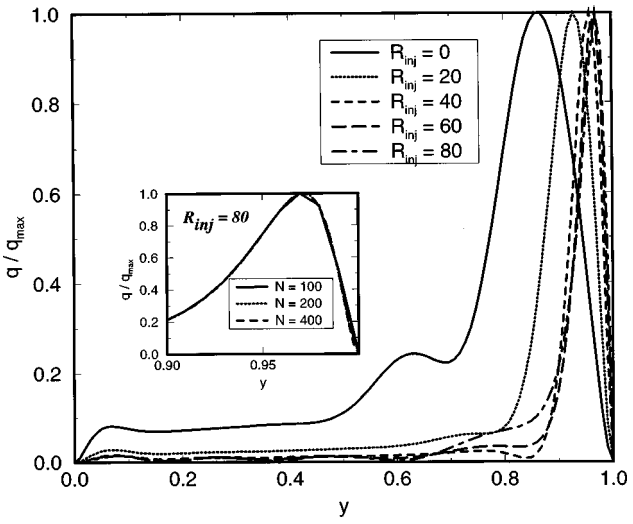

FIG. 8. Mean-kinetic-energy profiles for mode (b). For each R_{inj}, q has been scaled by its maximal value. Note that the shift towards the upper boundary is limited due to the no-slip condition imposed at $y=1$. The exaggerated area shows that a discretization using 100 points is sufficient to compute the corresponding eigenvector.

In definition (46), u and v are the real parts of the velocity fluctuations in the x and y directions, respectively,

$$u = \mathrm{Re}[\phi'(y)e^{i\alpha x}], \tag{47}$$

$$v = \mathrm{Re}[-i\alpha\phi(y)e^{i\alpha x}]. \tag{48}$$

$q(y)$ is thus calculated from

$$q = \frac{1}{4}(|\phi'|^2 + \alpha^2|\phi|^2). \tag{49}$$

In each graph, the wave number α and the outer Reynolds number R_o are fixed ($R_o = 3000$ and $\alpha = 1$), while the injection Reynolds number varies from 0 to 80; for each R_{inj}, q has been scaled by its maximal value. In Fig. 7, we have marked with a circle the profiles that have a *positive* expansion rate (i.e., which are *unstable*).

Mode (a) is such that most of the energy is contained in the lower half of the domain ($0 < y < \frac{1}{2}$) when no injection occurs (see Fig. 7). The q profile is characterized by two peaks (the first one located at $y_{a1} \simeq 0.15$, the second one at $y_{a2} \simeq 0.4$). Due to injection, the secondary maximum of q develops. It is shifted towards the upper boundary much faster than the primary peak: y_{a2} passes from 0.4 to 0.9 when R_{inj} increases from 0 to 80; at the same time, y_{a1} roughly passes from 0.15 to 0.20. Moreover, the value of the secondary peak is a quarter of the value of the primary peak for $R_{\mathrm{inj}} = 0$; this ratio is greater than 0.8 for $R_{\mathrm{inj}} = 80$.

Most of the kinetic energy of mode (b) is contained between $y = \frac{1}{2}$ and 1. Because eigenvectors (a) and (b) are symmetric about $y = \frac{1}{2}$ when $R_{\mathrm{inj}} = 0$, the positions of the two main energy peaks of mode (b) are $y_{b1} \simeq 0.85$ and $y_{2b} \simeq 0.6$ (see Fig. 8). When injection occurs, the primary peak is shifted towards the upper wall, but cannot reach this because of the no-slip condition at $y = 1$. The secondary peak is shifted too, but cannot develop [as it does in the (a) mode case] because of the existence of the primary peak. Its position does not change to a large extent and its contribution to the total kinetic energy of the mode decreases. The exaggerated part of this figure shows that the corresponding eigenvector is well resolved if 100 points are used to discretize Eq. (13). Indeed, no change is observed in the shape of the primary peak (expected to be the most difficult part to assess numerically) for this mode if 200 or 400 points are used instead.

For $R_{\mathrm{inj}} > 100$, mode (a) is such that the amount of energy contained in the range $\frac{1}{2} < y < 1$ is equivalent to that contained in the range $\frac{1}{2} < y < 1$. The value of the right peak (referred to above as the secondary peak) is now greater than that of the primary peak. It may be noted in Fig. 9 that mode (a) now follows a similar evolution to that of mode (b) for lower injection rates. The right peak cannot be displaced due to the no-slip condition prescribed at $y = 1$. Moreover, the left peak is weakly displaced and decreases as injection increases. This mode becomes more and more stable when injection increases, as dose mode (b). Finally, mode (a) becomes stable again for $R_{\mathrm{inj}} \simeq 170$.

From the above description of the evolution of q, it seems that the stabilization that occurs for large injection rates is strongly linked to the no-slip condition imposed at the upper wall. It would seem that the transverse flow was overwhelming the hydrodynamic instability. The same scenario is proposed in [8] to explain the restabilization that occurs when the outward flow increases. Other computations with different types of upper wall boundary conditions will be necessary to conclude this point.

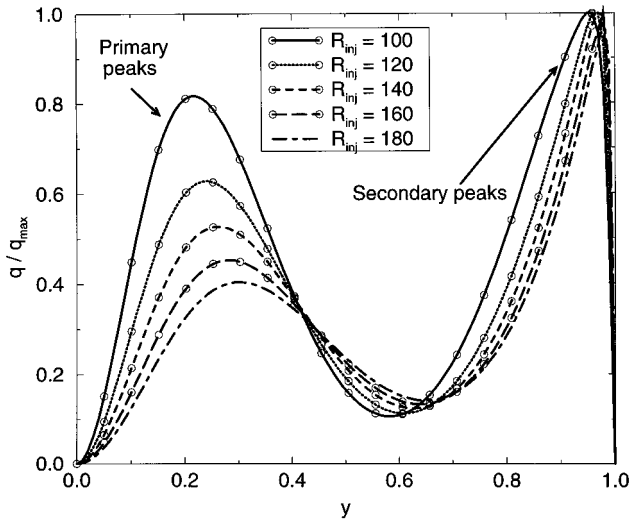

FIG. 9. Mean-kinetic-energy profiles for mode (a). Circles denote unstable modes. For each R_{inj}, q has been scaled by its maximal value. The right peak cannot evolve because of the no-slip condition imposed at $y = 1$ and the left peak decreases as R_{inj} increases.

C. Marginal stability of the generalized Couette flow

The previous description of mode evolution in the (c_r, c_i) plane suggests that it is possible to reach linear instability provided the injection Reynolds number is sufficiently large. This is confirmed for a wide range of outer Reynolds numbers and wave numbers in Fig. 10, which shows the maximal expansion rate of a linear perturbation ($\gamma = \max\{\alpha c_i, \alpha \in [0,1]\}$) versus R_{inj} for various R_o. (For all the computed

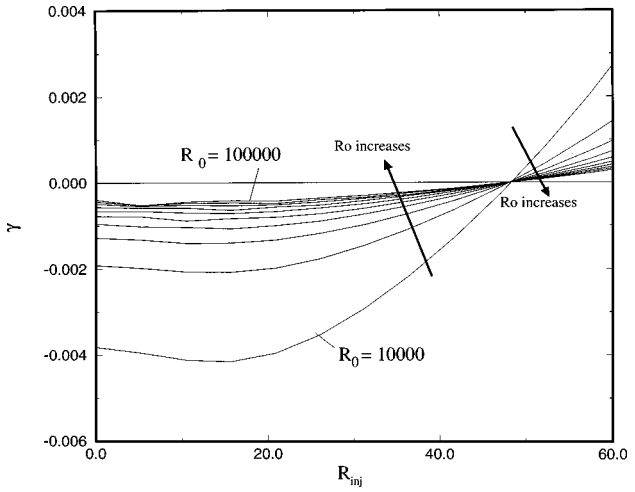

FIG. 10. Maximal expansion rate versus injection Reynolds number. The step in R_o is 10^4. This figure suggests that the value of R_{inj} for which the flow becomes unstable does not depend on the streamwise Reynolds number R_o.

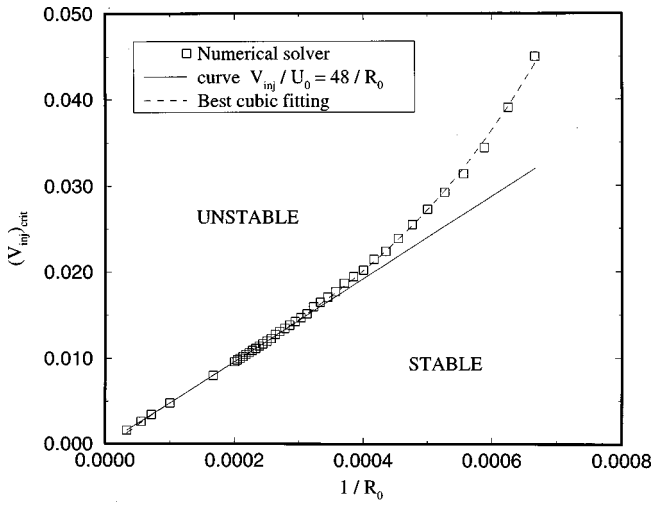

FIG. 11. Nondimensional critical injection velocity versus streamwise Reynolds number. For large streamwise Reynolds numbers R_o, the nondimensional critical injection velocity is a linear function of $1/R_o$. This implies that the critical injection Reynolds number $R_{\text{inj,crit}}$ is constant (see the text).

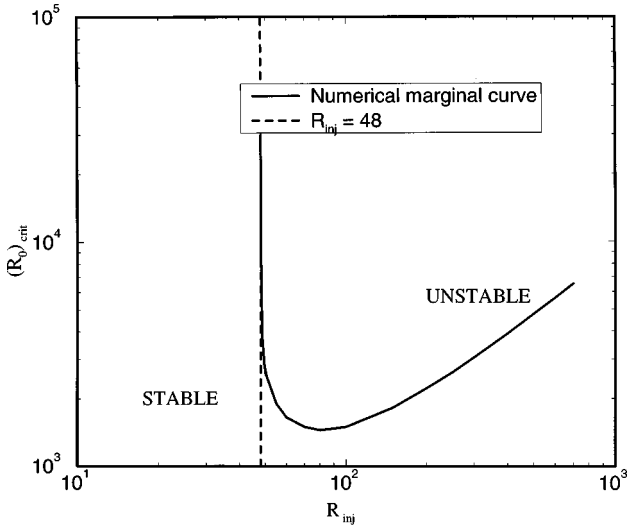

FIG. 12. Critical streamwise Reynolds number versus injection Reynolds number. As long as the injection Reynolds number is lower than its critical value 48, the Couette flow with injection and pressure gradient remains stable. Then injection destabilizes this base flow, which becomes conditionally unstable for $R_{\text{inj}}>48$. For values of R_{inj} greater than 80, the critical streamwise Reynolds number increases again.

values of R_o and R_{inj} we have checked that $\max\{\alpha c_i, \alpha \in [0,1]\} = \max\{\alpha c_i, \alpha \in [0,\infty]\}$.) Positive γ means that there exist $\alpha \in [0,\infty]$ for which the flow is unstable. As expected, for $R_{\text{inj}}=0$ the linear perturbation is damped for all α and R_o, in agreement with classical results on the stability of the Couette flow without injection and pressure gradient. With increasing R_{inj}, γ increases and becomes positive, so that the flow is linearly unstable. Moreover, a critical value of R_{inj} seems to exist, before which the flow remains linearly stable for all R_o. For higher R_{inj}, the flow becomes unstable: Wave numbers exist for which the perturbation grows, provided R_o is large enough. Figure 10 suggests that the value of R_{inj} for which the flow becomes unstable *does not depend on* R_o (at least for $10^4 < R_{\text{inj}} < 10^5$). The existence of a critical injection Reynolds number $R_{\text{inj,crit}}$ that does not depend on the streamwise Reynolds number R_o leads to the fact that the nondimensionalized injection velocity for which the flow becomes unstable ($V_{\text{inj,crit}}$) is an inverse function of the streamwise Reynolds number

$$V_{\text{inj,crit}} = \frac{V^*_{\text{inj,crit}}}{U_o} = \frac{C}{R_o} \tag{50}$$

with C positive constant. Figure 11 shows the marginal curve obtained by the numerical Orr-Sommerfeld solver plotted in the $(V_{\text{inj,crit}}, 1/R_o)$ plane and suggests $C \simeq 48$, at least for $1/R_o < 0.0003$. Then, since $V^*_{\text{inj,crit}}/U_o = R_{\text{inj,crit}}/R_o$, we obtain

$$R_{\text{inj,crit}} = C \simeq 48. \tag{51}$$

This value also corresponds to the intersection point of the curves γ versus R_{inj}, which are plotted in Fig. 10. For $1/R_o > 0.0003$, the slope of the curve plotted in Fig. 11 becomes greater and greater. In this range of streamwise Reynolds number, a cubic fitting provides a better approximation of $V_{\text{inj,crit}}$ as a function of $1/R_o$ (see Fig. 11). This means that for small values of R_o, the critical injection Reynolds number tends to increase. Consequently, 48 may be seen as a critical value for R_{inj}, under which the generalized Couette flow is always stable.

The existence of a critical injection Reynolds number may be interpreted by recalling that one can view the wall-injected flow as a mean flow with two components (U,V) and linearly perturb it to find its stability characteristics. This is the methodology used in this paper. Another approach would consist of viewing the Couette flow with injection and pressure gradient as a parallel Couette flow submitted to a perturbation (the injection and the associated pressure gradient). Since this latter flow is known to be stable for small disturbances, infinitesimal injection is expected to let the flow stable: Only injections with a sufficient momentum flux may lead to instability. As both approaches must be equivalent, we conclude that the critical streamwise Reynolds number (in the sense of the first approach) should remain infinite for all injection Reynolds number lower than a certain value. This is the main result of our numerical linear stability analysis: We find an injection Reynolds number of order 48, under which no instability occurs whatever the streamwise Reynolds number.

The critical streamwise Reynolds number has also been computed and is plotted versus R_{inj} in Fig. 12. This curve suggests that $(R_o)_{\text{crit}}$ remains infinite as long as $R_{\text{inj}} < 48$, in agreement with Fig. 11. For $R_{\text{inj}} > 48$, the critical streamwise Reynolds number drastically decreases to finite values. Its minimum value is around 1450 and is achieved for an injection Reynolds number of order 80. For larger R_{inj} the marginal streamwise Reynolds number increases. The same behavior has been found by Varapaev and Yagodkin [6] for their channel with injection at both sides.

VII. CONCLUSION

The stability of plane Couette flow submitted to wall injection through the lower wall and suction through the upper one has been examined numerically and asymptotically. The dispersion relations proposed by Davey [11] are generalized for small injection rates. These asymptotic relations show a linear dependence of the phase velocity with the injection Reynolds number. This behavior has been confirmed using a finite-difference numerical solver for the extended Orr-Sommerfeld equation. Moreover, the different constants of the asymptotic model have been obtained by fitting several numerical results. Injection is then found to have a destabilizing effect, as it linearly increases (for small injection Reynolds numbers) the expansion rate of small sinusoidal perturbations.

High injection rates are found by numerical computations to stabilize the flow, as the critical streamwise Reynolds number (which decreases for small injections) increases for $R_{\mathrm{inj}}>80$. Such a behavior has also been observed for channel flows [6] as well as for the Taylor-Couette flow [8]. The comparison of kinetic-energy profiles for different modes and different injection Reynolds numbers shows that the stabilization of the flow for high injection rates could be linked to an overwhelming effect due to the existence of the upper wall.

Due to injection, the eigenvalues are spread out in the (c_r, c_i) plane and the spectrum is no longer symmetric. In the same plane, and for increasing injection Reynolds numbers, the examination of certain paths shows the existence of nonlinear dependences between the phase velocities of the corresponding modes and R_{inj}. However, this does not seem to occur for low injection rates, in agreement with the asymptotic dispersion relations.

Finally, a critical injection Reynolds number exists below which no instability occurs. Our numerical solver suggests $R_{\mathrm{inj,critic}}\simeq 48$ for $R_o>3300$. This behavior may be simply described in the statement that classic parallel Couette flow is a linearly stable flow, so that a finite-momentum injected flux is required to destabilize it. A nonlinear analysis of plane Couette flow perturbed by a uniform finite injection would be useful to understand the behavior of the flow near this critical injection Reynolds number.

ACKNOWLEDGMENTS

We are grateful to Professor O. Thual and Dr. T. Poinsot for their support, Dr. Mangiavacchi and Dr. Rieutord for interesting discussions, and Dr. Vassilicos and Dr. Rudgyard for their remarks.

[1] F. Nicoud, *Eonctionnement des Moteurs à Propergol Solide Segmentés pour Lanceurs Spatiaux* (CNES-ONERA Paris, 1995).
[2] F. Vuillot, J. Propulsion Power **11**, 626 (1995).
[3] T. Cebeci, AIAA J. **8**, 2152 (1976).
[4] U. Piomelli, P. Moin, and P. Fertziger, Thermophys. **5**, 124 (1991).
[5] Y. Sumitani and N. Kasagi, AIAA J. **33**, 1220 (1995).
[6] V. Varapaev and V. Yagodkin, Izv. Akad Nauk SSSR Mekh. Zh. Gaza **4**, 91 (1969).
[7] T. S. Chang and W. K. Sartory, J. Fluid Mech. **27**, 65 (1967).
[8] K. Min and R. M. Lueptow, Phys. Fluids **6**, 144 (1994).
[9] D. Acheson, *Elementary Fluid Dynamics* (Clarendon, Oxford, 1990).
[10] W. H. Reid, *Basic Developments in Fluid Dynamics* (Holt, New York, 1965).
[11] A. Davey, J. Fluid Mech. **57**, 369 (1973).
[12] A. Berman, J. Appl. Phys. **24** (1953).
[13] P. Drazin and W. Reid, *Hyrodynamic Stability* (Cambridge University Press, Cambridge, 1981).
[14] S. Orszag, J. Fluid Mech. **50**, 689 (1971).
[15] K. Lele, J. Comput. Phys. **103**, 16 (1992).
[16] F. Nicoud, T. Poinsot, and H. Ha Minh, in *Proceedings of the Tenth Symposium on Turbulent Shear Flows* (Pennsylvania State University, 1995).
[17] D. D. Joseph, J. Fluid Mech. **33**, 617 (1968).